POSS@TiCl₄ Nanoparticles: A minimalism styled Ziegler-Natta Catalytic System

Wei Li[a,c]*, Chuanding Dong[a,c]*, Xiaodong Wang[b], Jingdai Wang[a,c], Yongrong Yang[c]

a. Ningbo Research Institute, Zhejiang University, Ningbo 315100, P.R. China

b. Chemical Engineering, School of Engineering, Lancaster University, Lancaster LA1 4YW, United Kingdom

c. Zhejiang Provincial Key Laboratory of Advanced Chemical Engineering Manufacture Technology, School of Chemical and Biochemical Engineering, Zhejiang University, Hangzhou 310027, Zhejiang, P. R. China

Corresponding Author: Wei Li: liwei2021@zju.edu.cn; Chuan-ding Dong, chuanding.dong@gmail.com

ABSTRACT

Heterogeneous catalysis plays a crucial role in industrial olefin polymerization. Mechanistic understanding and optimization of Ziegler-Natta (ZN) catalyst are limited by the considerable complexity resulting from the multiple ingredients and complicated structures. Re-designing ZN catalytic systems with reduced complexity and adequate performance is of great interest. Here, we show that self-assembled polyhedral oligomeric silsesquioxane (POSS)@$TiCl_4$ nanoparticles can effectively immobilize $TiCl_4$ molecules in n-heptane solution, achieving the exceptional utilization of active centres. This uncomplicated system exhibits heterogeneous-like catalytic performance in ethylene polymerization, featured by high activities, fouling-free polymerization and a series of desirable properties of the nascent polymers such as reduced entanglement and spherical morphology. In addition, these catalytic nanoparticles show robust resistance to H_2, and enhanced incorporation of comonomer towards ethylene/1-hexene copolymerization. By using DFT calculations the possible structures of the Ti active centres are proposed, of which a flexible double-Ti structure coordinated to Si-O-Si shows the most reduced energy barrier for ethylene insertion.

Key words: Heterogeneous polymerization catalysts; core-shell-corona; DFT calculations; polyethylene; Ziegler-Natta catalyst

1. Introduction

Polyethylene is an integral part of daily life. The capacity of polyethylene production and total polyethylene market value were more than 100 million tons and $200 billion in 2022, respectively[1-5]. In the industrial ethylene polymerization process (e.g., slurry or gas-phase polymerization), heterogeneous catalysts are widely employed thanks to their desirable performances in stabilizing the active species, avoiding the formation of reactor fouling, and directing the microstructure and particle morphology of polyethylene. [6,7]

Generally, these heterogeneous catalysts are obtained by the heterogenization of transition metal component as a promising strategy of robustly bonding the homogeneous catalyst with industrially preferred supports via covalent bonds, ion pairs or hydrogen bonds.[8-9] In the pursuance of high catalytic activity and flexible regulation on the structure and morphology of the synthesized polymers, advanced heterogeneous catalysts have been developed and optimized over decades.[8-10] The milestone of commercial Ziegler-Natta catalysts for ethylene polymerization is the utilization of microcrystalline $MgCl_2$ as support for the Ti species, since it is isomorphous with $TiCl_3$ and therefore leads to an excellent robust adsorption and well distribution of active species through the formation of Mg-Cl-Ti bridge[11]. Polyethylene with tailored chain structure can be synthesized by these $MgCl_2$-based Ziegler-Natta catalysts with considerable activity, where the removal of catalyst residual is no longer required in industry. In an industrial polymerization process, these highly activated catalytic units (i.e., microcrystalline $MgCl_2$ anchored Ti species) must be embedded or synthesized inside the spherical and porous carriers such as spherical $MgCl_2$

3

particles and silica, which determines the shape and size of the polyethylene particles and realizes the "drop-in" technology. [12,13] However, it should be mentioned that chemical reaction of $TiCl_4$ to the Si-OH groups of the silica cannot provide the required activity. [13,14] To this end, the modifiers, such as MgR_2, $Mg(OR)_2$, MgR_2/AlR_3 and Grignard reagents $RMgX$ (X=Cl or Br), have to be used as the Mg source for synthesizing the Mg compounds in the pores of calcined silica through the reaction with Si-OH groups. [10,13] This not only makes the synthesis procedure of heterogeneous Ziegler-Natta catalyst rather complicated, but results in a quite complex physical and chemical environment around the active centers: (*i*) the anisotropic transfer of reactants (e.g., ethylene, cocatalyst) inside the porous carrier creates various microscopic zones with different local atmosphere around the active species; [10-12] (*ii*) both Mg_{4c}^{2+} and Mg_{5c}^{2+} sites are the activated positions for anchoring transition metal component and electron donors, where multiple active centers are inevitably generated due to their mutual interaction. [15,16] Such complex microscopic environment makes mechanistic standpoint certainly far from perfect, and the optimization of Ziegler-Natta catalyst is still in a trial-and-error fashion so far. [7,17] Therefore, to simplify the catalyst heterogenization and demonstrate the intrinsic relationships between the structure of potential active species and catalytic performance are both significant and challenging.

Assembling catalytic molecules into nano-structures can reform catalyst systems and open a wide range of possibilities in controlling the distribution and properties of active sites. This strategy has gained numerous successes in the catalysis processes of environmental, energy, biological and molecular industries/technologies [19,20]. In this regard,

the nanoparticles are promising platforms for supporting catalytic molecules. Polyhedral oligomeric silsesquioxane (POSS) has a cubic inorganic Si_8O_{12} core surrounded by eight organic corner groups. Resembling surface feature of silica, incompletely condensed POSS with the size around 1-3 nm (e.g., one POSS molecule with 2 or 3 -OH) have also been extensively studied as homogeneous model support for silica-grafted catalysts. [21] The silsesquioxane were introduced on group 4 metals (Ti, Zr) as the ligands by either chloride metathesis or protonolysis. [22-23] In this way, Ti, Zr and Hf species chemically bonded to the hydroxyl of POSS could present the reasonable activity toward ethylene polymerization. However, the steric hindrance of POSS ligand influenced the catalytic performance and the chain growth procedure. The metal catalyst coordinated with the soluble POSS even behaved as the homogeneous catalysis. [21-25] Recently, catalytic nano-cluster for olefin polymerization opens a new research direction in the design of nanoscaled heterogeneous catalysis. [26] The amphiphilic comonomers formed initially soluble ionic nanoclusters and served as the "seeds" to induce the polymer growth on the clusters. These heterogenization strategy was realized since the particle growth on the cluster caused subsequent precipitation. Thus, the spherical polymer particles with the size less than 1 μm was synthesized without causing reactor fouling. [26] The functional group of amphiphilic comonomers was aggregated inside the formed ionic cluster through hydrogen bonds, which prevented the strong interaction of ionic polar groups from poisoning the metal center. [26]

These facts promote us to reconsider the design of heterogeneous catalysts for

ethylene polymerization. A flexible and simple immobilization strategy is desirable, which on one hand structurally stabilizes the active species, and on the other hand endows the ability to tailor the microstructure and morphology of the synthesized polymer with a considerable catalytic activity. The low-dimensional nanomaterials could be interesting candidates for such a supporting material.[27,28] In this work, we demonstrate this innovative concept to design heterogeneous catalysts toward ethylene polymerization based on POSS molecules. The O atom of chemical inert Si-O-Si cage in the POSS has been employed as an electron-rich site[29] to anchor catalytic molecules, which is aiming to stabilize and disperse the $TiCl_4$ active species and tailor the molecular architecture of synthesized polymer according to the self-assembly of POSS and $TiCl_4$ molecules. The assembled POSS@$TiCl_4$ unit exposes the active species on the POSS cages, which facilitates the contact and activation of cocatalyst. After capturing the $TiCl_4$, the amphiphilic POSS@$TiCl_4$ unit is purposed to form the certain nanoparticles in the *n*-heptane by the secondary aggregation, which endows the ability to tailor the entangled state and morphology of nascent polyethylene. We demonstrate that the catalysts exhibit unprecedented activities and produce nascent polyethylene with well-controlled architecture and morphology owing to the formation of robust but flexible active structures. Mechanistic understanding and catalyst optimization are illustrated *via* catalyst characterization and density functional theory (DFT) calculations.

2. Materials and methods

2.1 Materials

Disilanolisobutyl POSS (denoted as POSS) and oct-POSS (without -OH) was purchased from Hybrid Company (USA) and dried for 24 h before use (See **Figure S1**). Titanium (IV) chloride (TiCl$_4$, 99.9 wt%), triethylaluminium (TEAl, 1 mol l^{-1} in hexane) and *n*-heptane (99.9% wt%) were purchased from J&K Chemical Corp (China). The commercial MgCl$_2$/TiCl$_4$ catalyst with a Ti loading of 3.45 wt% was supplied by Sinopec Shanghai (China), which was used as a benchmark. *n*-heptane was distilled over sodium/diphenyl ketone before use. Polymerization-grade ethylene and nitrogen were obtained from Fangxin Corp. (China) and purified by filtering through Mn zeolite and subsequent zeolite of 5 Å. All operations on air-sensitive and moisture-sensitive compounds were conducted under an inert nitrogen atmosphere using standard Schlenk techniques or in a glovebox.

2.2 Catalyst Preparation

POSS (5 μmol) and TiCl$_4$ (900 μmol) were mixed in 10 ml of *n*-heptane at 60 °C for 2 h, to obtain the POSS@TiCl$_4$-180 catalytic suspension with light yellow color. The molar ratio of POSS to TiCl$_4$ were varied (TiCl$_4$ fixed at 900 μmol) to synthesize other catalytic suspensions which were labeled as POSS@TiCl$_4$-X, X meaning the molar ratio of TiCl$_4$/POSS, *i.e.,* 20, 90, 180 and 320. Pure TiCl$_4$ catalytic suspension was prepared without the presence of any POSS.

2.3 Ethylene polymerization

Ethylene polymerization was carried out in a 1.0 l Buchi stainless steel autoclave reactor which was equipped with a mechanical stirrer and a temperature controller. The

reactor was heated above 110 °C under vacuum for more than 3 h and repeatedly purged with nitrogen before polymerization. Then, the reactor temperature was reduced to 60 °C for the reactions using POSS@TiCl$_4$-X. 500 ml of *n*-heptane was added to the reactor before polymerization. After the introduction of TEAl as the cocatalyst, 1 ml of the catalytic suspension was injected into the reactor. The polymerization was carried out under a continuous ethylene flow at 3 bar with a stirring rate of 450 rpm. The polymerization was typically proceeded for 15 mins (or 90 mins in the study of H$_2$ resistance). At the end of reaction, the autoclave was quickly vented. The synthesized product was precipitated and washed with acidified ethanol (5 wt% hydrochloric acid) and dried at 60 °C under vacuum for 12 h. Repeated reactions with different samples from the same batch of catalyst delivered raw data that were reproducible to within ±7 %.

2.4 Computational details

The density functional theory (DFT) calculations used TPSSh hybrid functional and cc-PVDZ basis set. Dispersion interaction correction was included by using Grimme's D3 scheme and Becke-Johnson damping function. The search of transition state used Berny algorithm and was confirmed by imaginary frequency. All the DFT calculations were performed by using Gaussian 16 package. Multiwfn software was used for Hirshfeld charge analysis and calculations of density of states (DOS). The ligands of POSS molecules were replaced by H atoms to reduce the computational cost. Oct-POSS (without -OH groups) was used for all the calculations to avoid the structural complexity.[30,31]

2.5 Characterization

The morphologies of the catalysts were observed using transmission electron microscopy (TEM, Tecnai F20, USA). One droplet of the catalytic suspension was added onto the copper screen, which was then dried in the glove box and used for TEM observation. The chemical composition and elemental distribution of the nanoparticles were measured by spherical aberration corrected scanning transmission electron microscope (Cs-corrected STEM, Titan Chemi STEM, FEI, USA) using the energy-dispersive X-ray mode (STEM-EDX). The preparation procedure of samples for the Cs-corrected STEM measurement was the same with that for the TEM measurement. The catalytic nanoparticles in the suspension were also analyzed by the optical microscope (AXIO Imager A2M, ZEISS). Importantly, the suspension must be carefully sealed in the quartz cell before the measurements. The sealed catalytic suspension was subsequently put in the cell of dynamic light scattering (Zetasizer 3000HSA, Malvern, UK) to measure the particle size distribution at room temperature.

X-ray photoelectron spectroscopy (XPS) measurements were performed by using Escalab 250Xi with Al Ka radiation as the X-ray source (300 W, 1486.3 eV). The vacuum chamber was about 5×10^{-9} Torr. The binding energy was calibrated to C 1s peak at 284.6 eV. The suspension was dropped on the copper sheet and then dried in the glove box. The dried catalysts were then transferred to the XPS measurement with the protection of nitrogen. For the ^{49}Ti nuclear magnetic resonance (NMR) spectra, 0.6 ml of catalytic suspension was isolated from water and oxygen, and then measured on a Bruker AC-80 400 MHz spectrometer at ambient temperature.

The morphology of the synthesized polymer was observed using a scanning electron microscopy (SEM, Hitachi S-4700, Japan). The samples were sputter-coated by Pt before the SEM measurement. The weight-average molar mass (M_w) and the molecular weight distribution (MWD) were measured by a gel permeation chromatography (GPC) at 150°C with a PL-GPC-220 instrument (Polymer Laboratories, Shropshire, UK). The molecular weight of standard polystyrene ranged from 1000-14,000,000 g·mol^{-1}. 1,2,4-trichlorobenzene was used as the solvent.

Rheological studies were performed on a strain-controlled rheometer (HAAKE III instrument) to analyze the entanglement density of nascent polymers. A disk of 20 mm diameter was compressed under 20 tons at 130 °C for 30 min and used in all rheological studies. The disk between the parallel plates of the rheometer was heated to 160 °C under a nitrogen environment to prevent thermo-oxidative degradation. After thermal stabilization at 160 °C, the rheology experiments were started. The dynamic amplitude sweep test was performed at a fixed frequency of 1 Hz to determine the linear viscoelastic regime. The dynamic time sweep test was performed to follow the entanglement formation at a fixed frequency of 1 rad/s and strain in the linear viscoelastic regime. [32]

3. Results and discussion

3.1 Ethylene polymerization at low cocatalyst/catalyst (TEAl/TiCl4) ratios

Homogeneous TiCl$_4$ catalyst and commercial MgCl$_2$/TiCl$_4$ (3.45 wt% Ti) exhibit negligible activity at the nominal Al/Ti molar ratio R = 5. These catalysts require significantly higher R = (800 and 200, respectively) to be active (**Table 1**, runs 1-4). The

synthesized POSS/TiCl$_4$-2 catalyst, where TiCl$_4$ reacts with the -OH group, (molar [Ti]/[POSS] = 2, 7.5 wt% Ti, mimicking a Si-OH material (e.g. SiO$_2$) supported TiCl$_4$ catalyst based on covalent bonds) exhibits no activity (Table 1, run 5), responses that is expected and consistent with the literature. [14,33] Remarkably, increasing Ti/POSS ratio to 20 resulted in a successful reaction with the notable activity (0.5×10^6 g PE (mol$_{Ti}$·h·bar)$^{-1}$) and quality of products, where the nominal Al/Ti molar ratio R was equal to 5 (**Table 1**, run 6). This indicates a high atomic efficiency for the proposed stabilization strategy, making POSS@TiCl$_4$ an unprecedented system.

The catalytic activity of POSS@TiCl$_4$ system could also vary with the composition of the nanoparticles (**Table 1**, runs 6-9), namely the molar Ti/POSS ratio. Tuning in this ratio from 20 to 180 could increase the activity by a factor of 3 (0.5 to 1.6×10^6 g PE (mol$_{Ti}$·h·bar)$^{-1}$). A higher Ti/POSS molar ratio of 320 was found to be detrimental to catalysis and resulted in an activity reduce to 0.7×10^6 g PE (mol$_{Ti}$·h·bar)$^{-1}$ with reactor fouling. The obtained activities are even comparable to those of MgCl$_2$ supported mononuclear Ti catalysts (*i.e.*, 0.1 wt% Ti, $0.7\text{-}2.0\times10^6$ g PE (mol$_{Ti}$·h·bar)$^{-1}$) [34]. The catalytic performance was also found to be dependent on R. Taking POSS@TiCl$_4$-180 as a representative case, $R = 5$ turns to be the optimal, where higher (20) or lower (2) R value is less favorable for the process (**Table 1**, runs 10-12, **Figure S2**). This is due to the balance between the activated numbers of Ti atoms and the transfer of growing polymer chain towards TEAl. Nevertheless, the entire operating R range considered for this new family of catalysts is substantially lower to those employed for traditional Ziegler-Natta catalysts

(*e.g.*, 60-200) [35-37]. Moreover, the polymerization using POSS@TiCl$_4$ did not result in any reactor fouling (**Figure S3**). Apart from the high activity, the polyethylene produced, depending on *R*, typically takes the form of discrete, free-flowing and millimeter-sized spheres (**Figure S3**). The polyethylene products also have molecular weights (*M$_w$*) higher than 1.0×10^6 g mol^{-1}, *i.e.*, ultra-high molecular weight polyethylene (UHMWPE, **Table 1** and **Figure S4**). The nearly unchanged molecular weight distribution (MWD, 6.0±0.3) suggests similar chemical environments of the active sites. More importantly, the substantially reduced nominal loading of cocatalyst and the fouling-free advantage indicate the robust immobilization of active sites in this POSS@TiCl$_4$ system. The polymerization reactions were also conducted by using oct-POSS@TiCl$_4$ nanoparticles, which demonstrated very similar catalytic behavior (e.g., activity, fouling-free, low *R*, similar *M$_w$* and MWD) to those of their counterpart with -OH (**Figure S5** and **Table S1**). This demonstrates that the hydroxyl of POSS may contribute to the self-assemble process through the hydrogen bonds but presents the ignored influence to catalytic performance of active species. The Si-O-Si cage of the POSS can stably anchored the activated Ti species.

3.2 Catalyst characterization, structure-performance relationship

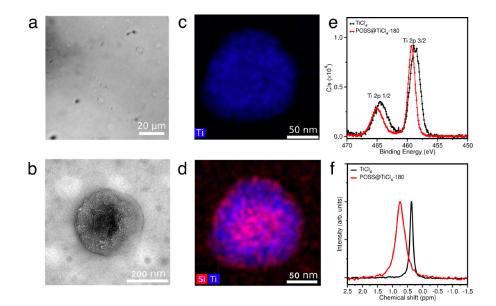*3.2.1 Characterization of catalyst structure and POSS-TiCl$_4$ interaction*

Figure 1. Structure of the synthesized POSS@TiCl₄ nanoparticles. (a) Optical microscope image of the POSS@TiCl₄-180 suspension; (b) TEM image of the nanoparticles formed in POSS@TiCl₄-180 suspension; (c) Ti (●) element distribution of the nanoparticle observed by the STEM-EDX mapping; (d) Si (●) and Ti (●) element distribution of the nanoparticle observed by the STEM-EDX mapping; (e) XPS comparison between POSS@TiCl₄ nanoparticles and pure TiCl₄; (f) ^{49}Ti NMR data of the POSS@TiCl₄ nanoparticles and pure TiCl₄

Prior to characterizing the catalysts, further control experiments were conducted to identify the catalytic components in the suspension. TiCl₄ suspension alone was tested (*i.e.*, in the absence of POSS, 90 μmol in 1 ml suspension), where significantly reduced activities (**Table S1**) with respect to the POSS@TiCl₄ suspension, as well as reactor fouling, were observed (**Figure S3**). The synthesized polyethylene exhibit a cocoon-like morphology without the presence of any particles (**Figure S3**), which is rather different from those

13

presented in Table 1, and indicates heavy leaching of active sites. In addition, the filtrate of POSS@TiCl$_4$-180 after sieving with 200 nm filter was also much less active than the original suspension (**Table S1**), suggesting a systematic characterization of the as-prepared suspension (typically 1 ml of *n*-heptane containing POSS and TiCl$_4$) was essential.

Taking POSS@TiCl$_4$-180 suspension as an example (nominal molar [Ti]/[POSS] = 180, 90 μmol TiCl$_4$ in 1 ml *n*-heptane), numerous particles in random motion were observed by using the optical microscope (**Figure 1a**). Representative TEM image (**Figure 1b**) shows that these particles, with an average size of *ca.* 225.2 nm (**Figure S6**), exhibit a core-shell-corona structure. STEM-EDX mapping further shows a homogeneous distribution of Ti atoms in the TiCl$_4$ cluster without the POSS (**Figure 1c**), while POSS and TiCl$_4$ molecules are enriched in the core and the outer shell, respectively (**Figure 1d**). A dispersed POSS corona was also observed in the surroundings of particles. The formation of such a structure is attributed to the thermodynamically favorable self-assembly and interactions of POSS and TiCl$_4$ molecules. [27,28] Such nanoparticles with numerous catalyst clusters are responsible to the exceptional activity and determine the spherical morphology of the synthesized polymer owing to the duplication effect (**Figure S3**). It is important to mention that, the formation of POSS@TiCl$_4$ nanoparticles rely much on the *n*-heptane solvent used, while in other solvent such as toluene the nanoparticles can easily collapse.

The interaction between POSS and TiCl$_4$ molecules was studied by X-ray photoelectron spectroscopy (XPS) (**Figure 1e**) and ^{49}Ti nuclear magnetic resonance (NMR) measurements (**Figure 1f**). In the XPS spectra of the nanoparticles, the peak of Ti 2*p* blue-

shifts *ca.* 0.5 eV (to 458.8 eV) with respect to the characteristic position of pure $TiCl_4$ (458.3 eV). The NMR measurement shows that, the chemical shift of ^{49}Ti rises from 0.4 to 1.0 ppm for the POSS@$TiCl_4$ suspension, suggesting a more pronounced electron deficiency of Ti atoms. The broaden ^{49}Ti NMR resonance of the POSS@$TiCl_4$ suspension further demonstrates the reduced mobility of $TiCl_4$ in the solution thanks to the presence of POSS molecules. In addition, these observations and measurements show similar resonance in the presence of POSS molecules with and without -OH groups (See **Figure S7**), where the considerable interaction between the Si-O-Si edge and $TiCl_4$ molecules are found and contribute to their similar catalytic performance. The contact between Si-O-Si edge of POSS and $TiCl_4$ is also addressed by DFT calculations. It is found that, when multiple $TiCl_4$ are in the vicinity of a POSS molecule, two typical Ti-O distances can be clearly identified around 3.4 Å and 2.5 Å, corresponding to the calculated binding energies (BE) around 0.40 eV and 0.50 eV, respectively (**Figure S8a**). Moreover, the latter case, namely the relatively stronger POSS-$TiCl_4$ binding, can further lead to the formation of $TiCl_4$ aggregations of small sizes bonded to POSS (POSS-$(TiCl_4)_4$-C in **Figure S8a**), where the Ti *2p* orbitals shift to deeper energies with respect to those of the structures without $TiCl_4$ aggregation (**Figure S8b**). This shows coincidence with the Ti-*2p* XPS data (**Figure 1e**).

Both the observations and the calculated results indicate that the coordination between Ti and Si-O-Si edge, even though weaker than a typical Ti-O covalent bond, can help sustaining the POSS@$TiCl_4$ nanoparticles. As a support material, the POSS molecule

15

significantly reduce the structural complexity of heterogeneous catalyst. As we show in **Table S2** and discuss in section 3.3, the electron-rich O atoms can transfer the electron to the activated Ti atoms and thus robust anchoring the Ti species. This could on the one hand tailor the catalytic performance and on the other hand help reducing the complexity in the system.

3.2.2 Correlation between catalytic activity and [Ti]/[POSS] ratio

POSS@TiCl$_4$ nanoparticles of varying [Ti]/[POSS] ratios and sizes can be obtained by changing the nominal molar ratio of TiCl$_4$ and POSS in the preparation, all with core-shell-corona structures (see **Figure S9** for STEM-EDX mapping and **Figure S6** for size data). The variation of the composition of the nanoparticles with the nominal molar ratio are shown in **Figure 2a**. The immobilization efficiency (*i.e.,* the actual amount of Ti immobilized by POSS over the total Ti feed) reaches the minimum for POSS@TiCl$_4$-180 (**Figure 2b**), measured by both bulk and surface [Ti]/[Si] ratios. This lowest efficiency however promotes the formation of a clearer core-shell-corona structure with the best TiCl$_4$ dispersion and accordingly the highest activity. The POSS-only suspension in *n*-heptane (without TiCl$_4$) was subsequently investigated, where an enhanced self-nucleation of the POSS molecules was observed at increasing POSS loadings (**Figure S10**). A competition between POSS self-nucleation, intermolecular self-assembly of TiCl$_4$ and POSS (required) therefore seems to be present, where the balance can be tuned by the relative amounts of POSS and TiCl$_4$.
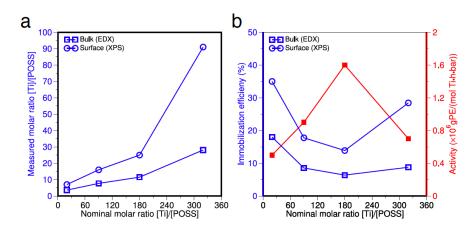
Figure 2. Correlation between structural compositions and performance of POSS@TiCl₄ catalyst. (a) Measured molar ratio [Ti]/[POSS] on the surface and in the bulk of the nanoparticles; (b) Catalytic activity and immobilization efficiency as function of the nominal molar ratio of [Ti]/[POSS].

Given the above observation of the catalytic suspension, a feasible methodology to enhance catalytic activity can be proposed. Since the catalyst preparation process is highly dependent on the aggregation of POSS molecules, the growth of POSS aggregates can be controlled by limiting the amount added per feed. POSS (5 μmol) was intermittently added into POSS@TiCl₄-180 catalytic suspension (10 ml *n*-heptane containing 900 μmol TiCl₄ and 5 μmol POSS) for 8 further times with an interval of 1 h between feeds. Overall, this procedure brought the [Ti]/[POSS] ratio down to 20. The catalytic activity of the resulted suspension was significantly increased to 1.9×10^6 g PE $(mol_{Ti} \cdot h \cdot bar)^{-1}$, equivalent to ~4 times of that obtained by the original POSS@TiCl₄-20 under identical reaction conditions (**Table 2**, run 3). This enhancement of activity clearly indicates that this intermittent addition of POSS optimizes the uptake of TiCl₄ molecules into highly active POSS@TiCl₄

17

species, verified by optical microscope observation (**Figure S11**). STEM-EDX analysis further confirmed that these newly formed nanoparticles exhibit the same composition as the original POSS@TiCl$_4$-180 nanoparticles (*i.e.*, measured [Ti]/[POSS] = 22, **Figure 2a**).

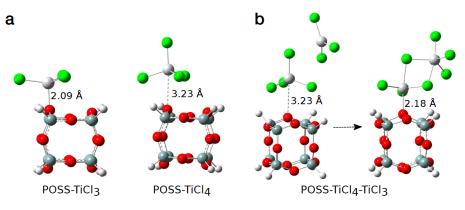*3.3 Elucidation of the catalytic structure and mechanism by DFT calculations*

Figure 3. Ti(III)'s binding to POSS (a) Optimized structures of POSS-TiCl$_3$, in comparison with POSS-TiCl$_4$. (b) Initial (left) and final (right) structures of POSS-TiCl$_4$-TiCl$_3$ optimization. The cage structure denote as the POSS molecular, where the red ball and gray ball indicate the O atoms and Si atoms, respectively. Ti atoms and Cl atoms are with white and green color, respectively.

The correlation between catalytic activity and the [Ti]/[POSS] molar ratio, as demonstrated in **Figure 2**, further evidences that the close contact between POSS and Ti species can directly impact on the catalytic reactions. To elucidate the underlying mechanism, the formation of Ti active centers and the role of POSS therein are of central importance. It is natural to probe the microscopic structures formed by POSS and Ti (III)

species by using DFT calculations, since the catalytic activity is known to be mainly contributed by Ti(III) species formed after co-catalyst activation of Ti(IV).

To this end, we consider the model clusters POSS-TiCl$_3$ for the direct contact conformation, and POSS-TiCl$_4$-TiCl$_3$ which represents the interaction of POSS and Ti(III) intermediated by TiCl$_4$. **Figure 3(a)** shows the optimized POSS-TiCl$_3$ structure, where the Ti-O coordination distance is significantly shorter than in POSS-TiCl$_4$ and is consistent with the stronger calculated BE. In comparison, the POSS-TiCl$_4$ interaction is weaker due to the less open structure around Ti atom. Nevertheless, with the presence of one TiCl$_3$, the interaction between TiCl$_4$ and POSS can be substantially enhanced. As illustrated in **Figure 3(b)**, the TiCl$_3$'s binding to a POSS-TiCl$_4$ in vicinity is directly driven by energetic advantage and leads to dramatic change of the original POSS-TiCl$_4$ structure. Notably, the Ti-O distance is shortened to a length (2.19 Å) close to that in POSS-TiCl$_3$ (2.08Å) in the optimized structure. These results indicate that the catalytic active Ti(III) can be immobilized not only directly by POSS, but also by POSS-TiCl$_4$, forming a double-Ti structure. A depiction of the electronic structures of POSS-TiCl$_3$ and POSS-TiCl$_4$-TiCl$_3$ is provided in **Figure S12**, which demonstrates the impact of POSS on the electronic states of Ti species. In particular, as shown in **Table S2**, there is a considerable charge transfer between POSS and Ti (III) species, implying the electron donor effect of POSS molecule. The charge transfer can be attributed to the coordination between the electron-rich O atoms and the Ti(III) cation in POSS-TiCl$_3$. Moreover, the situation in POSS-TiCl$_4$-TiCl$_3$ is similar, because the structural change therein renders the Ti coordinating to Si-O-Si

(originally a Ti(IV)) an unpaired electron and thus a behavior close to a Ti(III), as shown in **Figure S12b**.
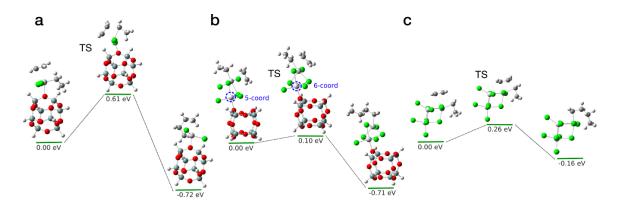

Figure 4. Catalytic performance of POSS-supported Ti(III) species. The profiles of ethylene insertion reaction catalyzed by (a) POSS-TiCl$_3$ (b) POSS-TiCl$_4$-TiCl$_3$ (c) (TiCl$_4$)$_2$-TiCl$_3$. For each catalytic structure, the energetics as well as structures of initial state, transition state (TS) and final state are presented.

The catalytic properties of alkylized POSS-TiCl$_2$R and POSS-TiCl$_4$-TiCl$_2$R (R=C$_2$H$_5$) structures are examined in term of the energy barrier of the ethylene insertion. The double-Ti structure in POSS-TiCl$_4$-TiCl$_2$R shows a significantly reduced barrier of 0.1 eV (**Figure 4b**) upon ethylene insertion with respect to the barrier of 0.6 eV given by the POSS-TiCl$_2$R (**Figure 4a**). This explains the outstanding catalytic activity of POSS@TiCl$_4$-180, highlighting the importance of the double-Ti catalytic structure. Examination of the insertion process reveals that the key to the reduced barrier lies in the structural flexibility of the double-Ti center: upon the ethylene insertion on the Ti(III) site, the adaption of the

POSS-TiCl$_4$-Ti$_2$R structure renders alternation of the Ti(IV) atom from 5-coordination in the reactant to 6-coordination in the transition state (TS), which effectively stabilizes the TS. Consistently, the higher energy barrier with the single-Ti catalytic structure of POSS-TiCl$_2$R can be attributed to the lack of such a flexibility. In addition, we examined ethylene insertion at the other Ti site, namely alkylized Ti(IV) site of POSS-TiCl$_3$R-TiCl$_3$. The barrier turns out to be 0.29 eV due to the rigid conformation of the Ti directly bonded to POSS (**Figure S13a**). This implies a decent possibility of polymerization at this site as well as the multi-center nature of the double-Ti structure, which is in line with the relatively broad MWD resulted from the present catalytic systems.

We note that the proposed structures of POSS-TiCl$_3$ and POSS-TiCl$_4$-TiCl$_3$ as shown in **Figure 3**, in spite of their small sizes and relatively simple geometries, reflect already the fundamental aspects of the activated POSS@TiCl$_4$ system, such as the impact of POSS on Ti species and different coordination conditions of Ti(III). Therefore, this minimalism styled structure can be taken as the prototype of immobilized Ti(III)-Ti(IV) clusters of large sizes and/or more complicated structures for understanding their crucial role in the catalytic mechanism.

To shed some light in the catalytic performance of the suspension where the POSS@TiCl$_4$ clusters were filtered out, the ethylene insertion reaction on pure Ti aggregates is also addressed. The Ti aggregate is modelled by a (TiCl$_4$)$_2$-TiCl$_2$R cluster, where the catalytic site is supported by a relatively rigid structure of a TiCl$_4$ cluster, rather than by the POSS molecule (**Figure 4c**). With this structure, the ethylene insertion

overcomes an energy barrier of 0.26 eV, which should also lead to a decent catalytic activity and is in agreement with our polymerization results (**Table 1**). The cluster undergoes a modest structural distortion in the reaction process and does not show the altered coordination as in POSS-TiCl$_4$-TiCl$_3$. Another structure of (TiCl$_4$)$_2$-TiCl$_2$R exhibits similar catalytic behaviors (**Figure S13b**). DFT calculations show also that the free-standing double-Ti structure (TiCl$_4$-TiCl$_2$R) without the presence of extra POSS or the TiCl$_4$ molecule can also lead to quite a low barrier of 0.15 eV (**Figure S13c**), where the altered coordination is also found. This demonstrates the flexible conformation of active species (TiCl$_4$-TiCl$_2$R) is the key to enhance the ethylene insertion. More importantly, the O-Ti coordination between the POSS and TiCl$_4$ ensures this flexibility, since all the Cl atoms of the bonded Ti species are dispersed without the occupation by other molecules (e.g., the Ti-Cl-Mg bridge in the classical MgCl$_2$).

The possible origin of the low cocatalyst load for the POSS@TiCl$_4$ catalytic systems was also probed by DFT calculation. The calculated BEs between TEA and POSS are significantly larger than that between TEA and TiCl$_4$ (**Figure S14**). This indicates that the TEA molecules can be effectively gathered around POSS, which could facilitate the interaction between TEA and Ti species.

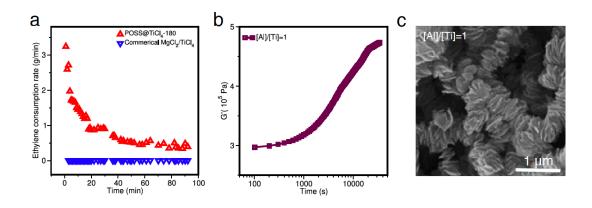*3.4 Features of the synthesized polymers and the Polymerization Process*

Figure 5. (a) Temporal variation of ethylene consumption rate over POSS@TiCl$_4$-180 and commercial MgCl$_2$/TiCl$_4$ catalysts (Polymerization in 7 bar H$_2$ and 3 bar C$_2$H$_4$, see conditions in **Table 2**); (b) Absolute values of the storage modulus (G') obtained on annealing the sample synthesized by POSS@TiCl$_4$-180 at $R = 1$; (c) SEM morphology of the polymer synthesized by POSS@TiCl$_4$-180 at $R = 1$.

3.4.1 High H$_2$ resistance

To examine the robustness of the new catalysts, POSS@TiCl$_4$-180 was also compared to a traditional MgCl$_2$/TiCl$_4$ catalyst under harsh reaction conditions, i.e., with high partial pressure of H$_2$. As can be seen from **Figure 5a**, the commercial catalyst does not possess any activity at $R = 5$ even in the absence of H$_2$, whereas the POSS-mediated system could keep a considerable consumption rate of ethylene (0.9 g min^{-1}) for over 90 mins at 7 bar of H$_2$ (with 3 bar of C$_2$H$_4$). By using the possible catalytic structures in **Figure 4** and **Figure S13**, we calculated the BEs of H$_2$ absorption on the catalytic sites. It turns out that the Ti(III) site of POSS-TiCl$_4$-TiCl$_3$ shows a relatively weak binding with H$_2$ (**Figure S15**), which is

in agreement with the polymerization observations and can be taken as a support for our proposed catalytic structures.

3.4.2 Enhanced comonomer effect

Particularly interesting is that, this catalyst also exhibits an excellent ethylene/1-hexene copolymerization property, where a considerable insertion ratio of 1-hexene are achieved during the slurry polymerization (i.e, 1.3 mol%, see **Figure S16**). [38] This finding provides possible approaches of simplifying the existing industrial processes, minimizing the use of co-catalyst and ultimately saving operational costs, which may be of great significance to the polymerization industry.[10,35]

3.4.3 Reduced entanglement of synthesized polyethylene

The weak entanglement of synthesized polyethylene, which decreases the molten viscosity and thus improves processability[39,40], is evidenced by molten rheology, where the modulus build-up curve shows a low starting value and takes a long time (*e.g.*, more than 3.6×10^4 s for the UHMWPE synthesized at $R = 1$) to reach the thermodynamically stable state (**Figure 5b**). These observations are consistent with an entanglement of nascent UHMWPE via distribution of active sites: with a lower nominal loading of TEAl (*e.g.*, $R = 1$), activated $TiCl_4$ molecules in the POSS systems are highly isolated, since the self-assembled core-shell-corona catalytic nanoparticles expose the numerous 'starved' precursor to the rare TEA molecule. This is favor to isolate the active sites and propagated chains, especially at the low cocatalyts loading, which reduces the chain overlap and the

entanglement in the nascent UHMWPE. This scattered distribution of active sites are further evidenced by the petaline-like structures in each grain of a UHMWPE particle due to the morphology duplication effect (**Figure 5c**).

4. Conclusions

In the present work, we demonstrate that the POSS-TiCl$_4$ nanoparticles self-assembled in n-heptane solution can show excellent catalytic performance towards ethylene polymerization, featured by the high catalytic activity comparable to industrial ZN catalysts, the reduced use of cocatalyst, a robust H$_2$ resistance and higher comonomer incorporation in polymerization, reduced entanglements and the desirable morphology of synthesized products. The catalytic performance can be influenced by the [Ti]/[POSS] nominal ratio and the self-assembling of POSS in preparation procedures.

Compared to MgCl$_2$-supported ZN catalysts, the complexity of the POSS-TiCl$_4$ catalytic system is substantially reduced because the robust immobilization of catalytic Ti species is achieved by the coordination with Si-O-Si edge. We propose several possible structures of catalytic sites, among which a double-Ti structure shows the lowest energy barrier for ethylene insertion owing to its structural flexibility. Moreover, the POSS@TiCl$_4$ catalytic system can be synthesized by simple mixing procedure and straightforwardly integrated to the polymerization process.

Data availability

Data will be made available on request.

Declaration of Competing Interest

Acknowledgments

Appendix A. Supplementary material

Supporting information for this article (including details on the related catalyst and polymer characterization) is given via a link at the end of the document.

References

[1] M. Stürzel, S. Mihan, R. Mülhaupt. From multisite polymerization catalysis to sustainable materials and all-polyolefin composites. Chem. Rev., 116 (2016) 1398-1433.

[2] M.A.A. AlMa'adeed, I. Krupa. Polyolefin Compounds and Materials Ch. 1, Springer, Heidelberg, 2016.

[3] T. J. Hutley, M. Ouederni. Polyolefin Compounds and Materials Ch. 2, Springer, Heidelberg, 2016.

[4] D. W. Sauter, M. Taoufik, C. Boisson. Polyolefins, a success story. Polymers, 9 (2017) 185.

[5] Y. Gao et al. Highly branched polyethylene oligomers via group IV-catalysed

polymerization in very nonpolar media. Nat. Catal., 2 (2019) 236-242.

[6] A. Alizadeh, T. F. L. McKenna, Particle Growth during the Polymerization of Olefins on Supported Catalysts. Part 2: Current Experimental Understanding and Modeling Progresses on Particle Fragmentation, Growth, and Morphology Development, Macromol. React. Eng., 12 (2017) 1700027.

[7] E. Morra, E. Giamello, S. Van Doorslaer, G. Antinucci, M. D'Amore, V. Busico, M. Chiesa, Probing the coordinative unsaturation and local environment of Ti^{3+} sites in an activated high yield Ziegler-Natta catalyst. Angew. Chem. Int. Ed., 54 (2015) 4857−4860.

[8] J. D. Pelletier, J. M. Basset, Catalysis by Design: Well-Defined Single-Site Heterogeneous Catalysts. Acc. Chem. Res., 49 (2016) 664−677.

[9] S. L. Wegener, T. J. Marks, P. C. Stair, Design strategies for the molecular level synthesis of supported catalysts. Acc. Chem. Res., 45 (2012) 206−214.

[10] M. Klapper, D. Joe, S. Nietzel, J. W. Krumpfer, K. Müllen, Olefin Polymerization with Supported Catalysts as an Exercise in Nanotechnology, Chem. Mat., 26 (2014) 802-819.

[11] T. F. L. McKenna, J. B. P. Soares, Single particle modelling for olefin polymerization on supported catalysts: A review and proposals for future developments. Chem. Eng. Sci., 56 (2001) 3931-3949.

[12] T. F. L. McKenna, A. Di Martino, G. Weickert, J. B. P. Soares, Particle Growth During the Polymerisation of Olefins on Supported Catalysts, 1-Nascent Polymer Structures.

Macromol. React. Eng., 4 (2010) 40−64.

[13] R. Hoff, Handbook of Transition Metal Polymerization Catalysts, Second Edition, Wiley, 2018.

[14] E. Groppo, K. Seenivasan, E. Gallo, A. Sommazzi, C. Lamberti, C. Barzan, Activation and In Situ Ethylene Polymerization on Silica-Supported Ziegler−Natta Catalysts, ACS Catal., 5 (2015) 5586-5595.

[15] E. Groppo, K. Seenivasan, C. Barzan, The potential of spectroscopic methods applied to heterogeneous catalysts for olefin polymerization. Catal. Sci. Technol., 3 (2012) 858-878.

[16] A. Correa, F. Piemontesi, G. Morini, L. Cavallo, Key Elements in the Structure and Function Relationship of the $MgCl_2/TiCl_4$/Lewis Base Ziegler-Natta Catalytic System. Macromolecules, 40 (2007) 9181−9189.

[17] M. D'Amore, R. Credendino, P. H. M. Budzelaar, M. Causá, V. Busico, A periodic hybrid DFT approach (including dispersion) to $MgCl_2$-supported Ziegler-Natta catalysts-1: $TiCl_4$ adsorption on $MgCl_2$ crystal surfaces. J. Catal., 286 (2012) 103-110.

[18] S.T. Hunt, M. Milina, A.C. Alba-Rubio, C.H. Hendon, J.A. Dumesic, Y. Román-Leshkov, Self-assembly of noble metal monolayers on transition metal carbide nanoparticle catalysts, Science, 352, (2016) 974-978.

[19] R. Ye, T. J. Hurlburt, K. Sabyrov, S. G. Alayoglu, A. Somorjai. Molecular catalysis science: Perspective on unifying the fields of catalysis. P. Natl. Acad. Sci. USA., 113 (2016) 5159-5166.

[20] Q. L. Zhu, Q. Xu. Immobilization of Ultrafine Metal Nanoparticles to High-Surface-Area Materials and Their Catalytic Applications. Chem, 1 (2016) 220-245.

[21] C. Calabrese, C. Aprile, M. Gruttadauria, F. Giacalone, POSS Nanostructures in Catalysis, Catal. Sci. Technol., 10 (2020) 7415-7447.

[22] R. Duchateau, H. C. L. Abbenhuis, R. A. van Santen, S. K. H. Thiele and M. F. H. van Tol, Half-Sandwich Titanium Complexes Stabilized by a Novel Silsesquioxane Ligand:? Soluble Model Systems for Silica-Grafted Olefin Polymerization Catalysts, Organometallics, 17 (1998) 5222-5224.

[23] R. Duchateau, U. Cremer, R. J. Harmsen, S. I. Mohamud, H. C. L. Abbenhuis, R. A. van Santen, A. Meetsma, S. K. H. Thiele, M. F. H. van Tol and M. Kranenburg, Half-sandwich group 4 metal siloxy and silsesquioxane complexes: soluble model systems for silica-grafted olefin polymerization catalysts, Organometallics, 18 (1999) 5447-5459.

[24] A. Mehta, G. Tembe, M. Bialek, P. Parikh, G. Mehta, Synthesis and catalytic studies of Ti-anchored disilanol isobutyl-POSS/alkylaluminum system, J. Mol. Catal. A-Chem., 361-362 (2012) 17-28.

[25] A. Mehta, G. Tembe, P. Parikh and G. Mehta, Catalytic ethylene polymerization by the titanium-polyhedral oligomeric silsesquioxane-$Et_3Al_2Cl_3$ systemReact. Kinet. Mech. Catal., 104 (2011) 369-375.

[26] C. Tan, C. Zou, C. L. Chen, An Ionic Cluster Strategy for Performance Improvements and Product Morphology Control in Metal-Catalyzed Olefin-Polar Monomer

Copolymerization, J. Am. Chem. Soc., 144 (2022) 2245-2254.

[27] L. J. Ren, H. K. Liu, H. Wu, M. B. Hu, W. Wang, Toward cluster materials with ordered structures via self-assembly of herocluster janus molecules. Adv. Mater., (2019) 1805863.

[28] S. E. Létant, A. Maiti, T.V. Jones, J. L. Herberg, R.S. Maxwell, A.P. Saab, Polyhedral oligomeric silsesquioxane (POSS)-stabilized Pd nanoparticles: factors governing crystallite morphology and secondary aggregate structure. J. Phys. Chem. C, 113 (2009) 19424-19431.

[29] W. Li, N. Wang, Y. Cao, X. Tang, C.D. Dong, A Robust Immobilization Strategy in the Nano-Dispersed Ziegler-Natta Catalyst: Non-covalent O-Ti Coordination. Chem. Comm., 56 (2020) 10843-10846.

[30] M. J. Frisch, G. W. Trucks, H. B. Schlegel, G. E. Scuseria, M. A. Robb, J. R. Cheeseman, G. Scalmani, V. Barone, G. A. Petersson, H. Nakatsuji, X. Li, Gaussian 16, Revision C.01, Gaussian Inc., Wallingford CT, 2016.

[31] T. Lu, F. Chen, Multiwfn: A multifunctional wavefunction analyzer, J. Comput. Chem. 33 (2012) 580-592.

[32] S. Rastogi, D.R. Lippits, G.W.M. Peters, R. Graf, Y.F. Yao, H.W. Spiess, Heterogeneity in polymer melts from melting of polymer crystals. Nat. Mater., 4 (2005) 635-641.

[33] R. Credendino, D. Liguori, Z. Q. Fan, G. Morini, L. Cavallo. Toward a unified model explaining heterogeneous Ziegler-Natta catalysis. ACS Catal., 5 (2015) 5431-5435.

[34] B. Jiang, Y. Weng, S. Zhang, Z. Zhang, Z. Fu, Z. Fan, Kinetics and mechanism of

ethylene polymerization with $TiCl_4/MgCl_2$ model catalysts: effects of titanium content. J. Catal., 360 (2018) 57-65.

[35] Böhm, L. L. The ethylene polymerization with Ziegler catalysts: fifty years after the discovery. Angew. Chem. Int. Ed., 42 (2003) 5010-5030.

[36] E. Y. Chen, T. J. Marks. Cocatalysts for metal-catalyzed olefin polymerization: activators, activation processes, and structure-activity relationships. Chem. Rev., 100 (2000) 1391-1434.

[37] P. Liang, W. Li, Y.M. Chen, C.D. Dong, Q. Zhou, Y.R. Feng, M. Chen, J.C. Dai, C.J. Ren, B.B. Jiang, J.D. Wang, Y.R. Yang. Revealing the Dynamic Behaviors of Tetrahydrofuran for Tailoring the Active Species of Ziegler-Natta Catalysts. ACS Catal., 11 (2021) 4411-4421.

[38] B. Jiang, X. Liu, Y. Weng, Z. Fu, A. He, Z. Fan, Mechanistic study on comonomer effect in ethylene/1-hexene copolymerization with $TiCl_4/MgCl_2$ model Ziegler-Natta catalysts, J. Catal., 369 (2019) 324-334.

[39] A. Pandey, Y. Champouret, S. Rastogi, Heterogeneity in the distribution of entanglement density during polymerization in disentangled ultrahigh molecular weight polyethylene. Macromolecules, 44 (2011) 4952-4960.

[40] Y. Chen, P. Liang, Z. Yue, W. Li, C. Dong, B. Jiang, J. Wang, Y. Yang. Entanglement Formation Mechanism in the POSS Modified Heterogeneous Ziegler-Natta Catalysts. Macromolecules, 52 (2019) 7593−7602.

Tables

Table 1. Ethylene polymerization at low cocatalyst/catalyst ratios (R).[a]

Entry	Catalyst	R	Activity[f]	M_w 10^4 (g mol^{-1})	MWD	^{49}Ti chemical shift (ppm)	Reactor fouling
1	Homo-TiCl$_4$[b]	800	1.0	–[g]	–	–	√
2	Homo-TiCl$_4$[b]	5	0.04	–	–	–	√
3	MgCl$_2$/TiCl$_4$[c]	5	0.02	–	–	–	×
4	MgCl$_2$/TiCl$_4$[d]	200	0.8	–	–	–	×
5	POSS/TiCl$_4$-2[e]	5	0	–	–	–	–
6	POSS@TiCl$_4$-20	5	0.5	173.5	5.9	0.6	×
7	POSS@TiCl$_4$-90	5	0.9	170.0	6.0	0.8	×
8	POSS@TiCl$_4$-180	5	1.6	149.7	6.1	1.0	×
9	POSS@TiCl$_4$-320	5	0.7	156.8	5.9	1.4	√
10	POSS@TiCl$_4$-180	20	0.7	130.6	6.3	1.0	×
11	POSS@TiCl$_4$-180	10	0.9	137.7	6.1	1.0	×
12	POSS@TiCl$_4$-180	2	1.2	153.7	5.7	1.0	×
13	POSS@TiCl$_4$-180	1	0.6	156.0	6.0	1.0	×

[a]Reaction conditions: 90 μmol TiCl$_4$, 15 mins, 500 ml n-heptane, 3 bar C$_2$H$_4$ and 60 °C;
[b]1 μmol TiCl$_4$;
[c]90 μmol TiCl$_4$, commercial catalyst with a Ti loading of 3.45 wt%;
[d]10 μmol TiCl$_4$;
[e]Ti loading of 7.5 wt%, nominal loading of Ti/POSS = 2;
[f]10^6 g (mol$_{Ti}$·h·bar)$^{-1}$ based on the nominal loading of Ti;
[g]'–' means not measured.

Table 2. POSS-inspired novel ethylene polymerization catalysts.[a]

Entry	Catalyst	R	Activity[e]	M_w $10^4 \, (\text{g mol}^{-1})$	MWD	Reactor fouling
1	POSS@Cp$_2$ZrCl$_2$[b]	40	0.7	18.4	2.8	×
2	POSS@Cat-Fe[b]	40	0.5	35.5	5.6	×
3	POSS@TiCl$_4$-20-B[c]	5	1.9	–[f]	–	×
4	POSS@TiCl$_4$-180[d]	5	0.1	26.1	5.4	×

[a]Reaction conditions: 90 μmol of transitional metal, 15 mins reaction time, 500 ml of *n*-heptane, 3 bar of C$_2$H$_4$ and 60 °C (30 °C for entry 2);
[b]The cocatalyst is MAO;
[c]POSS was added over 8 batches into the POSS@TiCl$_4$-180;
[d]in the presence of 7 bar H$_2$ and 3 bar C$_2$H$_4$, polymerization time of 90 mins;
[e]10^6 g (mol$_{Ti/Zr/Fe}$·h·bar)$^{-1}$ based on the nominal metal loading;
[f]'–' means not measured.